mTORC1 maintains renal tubular homeostasis and is essential in response to ischemic stress

Florian Grahammer[a], Nora Haenisch[b], Frederic Steinhardt[a], Lukas Sandner[a], Malte Roerden[b], Frederic Arnold[a], Tomke Cordts[a], Nicola Wanner[a,c,d], Wilfried Reichardt[e], Dontscho Kerjaschki[f], Markus A. Ruegg[g], Michael N. Hall[g], Pierre Moulin[h], Hauke Busch[i,j,k], Melanie Boerries[i,j,k], Gerd Walz[a], Ferruh Artunc[b,1], and Tobias B. Huber[a,c,l,1,2]

[a]Renal Division, University Medical Center Freiburg, 79106 Freiburg, Germany; [b]Renal Division, University Hospital Tübingen, 72076 Tübingen, Germany; [c]Spemann Graduate School of Biology and Medicine, [d]Faculty of Biology, [i]Institute of Molecular Medicine and Cell Research, and [l]Centre for Biological Signalling Studies, Albert Ludwigs University of Freiburg, 79104 Freiburg, Germany; [e]Department of Medical Physics, University Medical Center Freiburg, 79106 Freiburg, Germany; [f]Department of Pathology, University of Vienna, 1090 Vienna, Austria; [g]Biozentrum Basel, University of Basel, 4056 Basel, Switzerland; [h]Novartis Institutes for Biomedical Research, Preclinical Safety, Discovery and Investigative Safety, 4002 Basel, Switzerland; [j]German Cancer Consortium, 69120 Heidelberg, Germany; and [k]German Cancer Research Center, 69120 Heidelberg, Germany

Edited by Marilyn G. Farquhar, University of California, San Diego, La Jolla, CA, and approved June 2, 2014 (received for review February 7, 2014)

Mammalian target of rapamycin complex 1 (mTORC1) is a key regulator of cell metabolism and autophagy. Despite widespread clinical use of mTORC1 inhibitors, the role of mTORC1 in renal tubular function and kidney homeostasis remains elusive. By using constitutive and inducible deletion of conditional *Raptor* alleles in renal tubular epithelial cells, we discovered that mTORC1 deficiency caused a marked concentrating defect, loss of tubular cells, and slowly progressive renal fibrosis. Transcriptional profiling revealed that mTORC1 maintains renal tubular homeostasis by controlling mitochondrial metabolism and biogenesis as well as transcellular transport processes involved in countercurrent multiplication and urine concentration. Although mTORC2 partially compensated for the loss of mTORC1, exposure to ischemia and reperfusion injury exaggerated the tubular damage in mTORC1-deficient mice and caused pronounced apoptosis, diminished proliferation rates, and delayed recovery. These findings identify mTORC1 as an important regulator of tubular energy metabolism and as a crucial component of ischemic stress responses.

mTOR | mitochondrial biogenesis | acute kidney injury | tubular transport | urinary concentration mechanism

The kidney is the main regulator of body fluid and electrolyte homeostasis, using diverse types of transporters, channels, and pumps to modify the primary ultrafiltrate (1). Intracellular kinase networks regulating transport mechanisms are increasingly recognized as playing pivotal roles in orchestrating these energy-dependent processes (2, 3). Distinct tubular segments require an enormous amount of ATP to accomplish transcellular transport (4, 5). This need of ATP in turn necessitates a high mitochondrial density, particularly prominent in the proximal tubule and the thick ascending loop of Henle (6). Although central to energy metabolism, the role of mammalian target of rapamycin (mTOR) complexes in maintaining renal tubular homeostasis has not been thoroughly investigated in the kidney (7). Originally described in yeast, TOR is evolutionarily highly conserved (8–12). The mammalian homologs of TOR complex 1 (TOR1) and TOR complex 2 (TOR2), named "mTORC1" and "mTORC2," are intracellular multiprotein complexes consisting of six (mTORC1) and seven (mTORC2) known protein components (13). Their common backbone consists of the mTOR kinase, DEP domain-containing mTOR-interacting protein (DEPTOR), and mammalian lethal with Sec13 protein 8 (mLST8). In mTORC1, mLST8 interacts with regulatory associated protein of mTOR (RAPTOR) (11) and is sensitive to the mTOR inhibitor rapamycin, whereas the rapamycin-insensitive complex mTORC2 consists of mammalian stress-activated protein kinase-interacting protein (mSIN1), rapamycin-insensitive companion of mTOR (RICTOR), and proline-rich protein 5-like (PRR5L). mTORC1 integrates a wide variety of nutrient cues, including growth factors, amino acids, cellular energy content, and cellular stress. To regulate downstream events such as cellular growth, cell division, and cell metabolism, mTORC1 phosphorylates a diverse set of substrates (7, 14).

Inhibitors of mTORC1 are commonly used in solid-organ transplantation, and electrolyte abnormalities such as hypophosphatemia and hypokalemia have been reported repeatedly in patients treated with rapamycin, although no plausible pathophysiological concept explains these findings (15–18). Mice treated with rapamycin can develop a Fanconi-like proximal tubular injury pattern consisting of glucosuria, amino aciduria, and phosphaturia (19), whereas renal transplant patients receiving mTOR inhibitors early after transplantation experience increased rates of delayed graft function (20). A prolonged recovery after ischemia/reperfusion (I/R) injury also is observed commonly in animals treated with rapamycin (21). Despite the assumption that these perturbations are related to the direct effects of mTOR inhibitors on tubular epithelial cells in the kidney, it has been difficult to differentiate these findings from the systemic effects of mTOR inhibitors. Because mTOR inhibitors are used increasingly to treat various cancers as well as hereditary conditions (22–24), it is important to understand their impact on

Significance

Mammalian target of rapamycin complex 1 (mTORC1) inhibitors are commonly used as immunosuppressants in solid-organ transplantation and as antiproliferative agents in various cancers. Despite indications of serious renal adverse events caused by mTORC1 inhibition, the role of mTORC1 for renal epithelial function and homeostasis has remained elusive. Unexpectedly, tubular mTORC1 controls energy-driven urine-concentrating mechanisms by maintaining mitochondrial biogenesis. Under pathophysiological conditions, mTORC1-dependent mitochondrial biogenesis is essential for energy supply and adaptation in response to ischemia. These findings identify mTORC1 as an important regulator of tubular energy metabolism, transcellular transport processes, and ischemic stress responses.

Author contributions: F.G., F. Artunc, and T.B.H. designed research; F.G., N.H., F.S., L.S., M.R., F. Arnold, T.C., N.W., W.R., D.K., P.M., H.B., M.B., and F. Artunc performed research; M.A.R. and M.N.H. contributed new reagents/analytic tools; F.G., P.M., H.B., M.B., F. Artunc, and T.B.H. analyzed data; and F.G., G.W., F. Artunc, and T.B.H. wrote the paper.

Conflict of interest statement: T.B.H. received project-specific grant funding from Pfizer Pharma GmbH and has acted as a consultant for Abbott Pharma, Roche, Astellas, Genzyme, and Pfizer Pharma. P.M. is an employee of Novartis AG, Basel, Switzerland.

This article is a PNAS Direct Submission.

Data deposition: The data reported in this paper have been deposited in the Gene Expression (GEO) database, www.ncbi.nlm.nih.gov/geo (accession no. GSE54417).

[1]F. Artunc and T.B.H. contributed equally to this work.

[2]To whom correspondence should be addressed. E-mail: tobias.huber@uniklinik-freiburg.de.

This article contains supporting information online at www.pnas.org/lookup/suppl/doi:10.1073/pnas.1402352111/-/DCSupplemental.

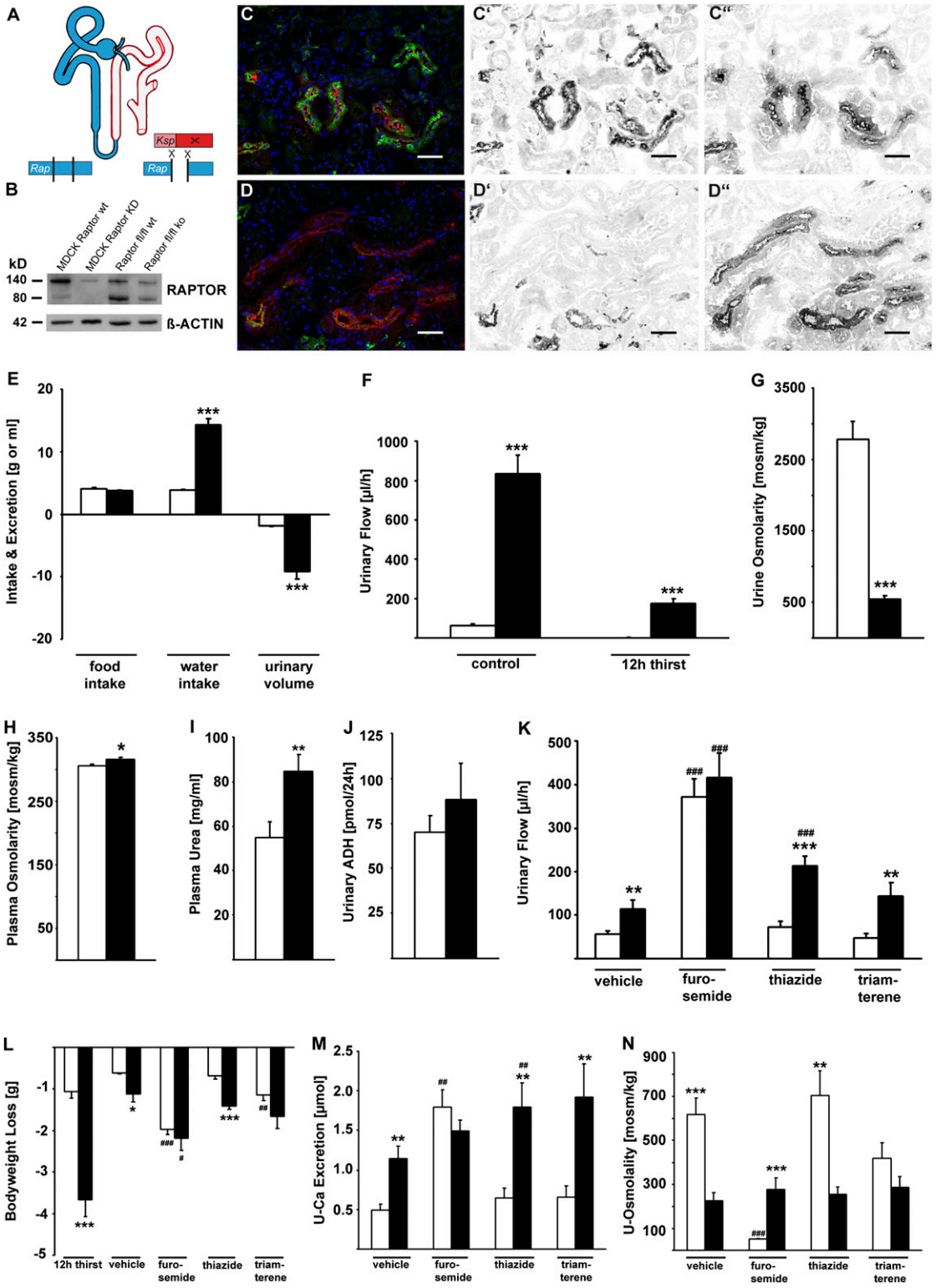

Fig. 1. Tubular cell-specific mTORC1 deletion leads to defective concentrating mechanisms and polyuria. (*A*) Schematic of the recombination strategy and the site of the *Ksp Cre*-mediated *Raptor* knockout within the tubular system. (*B–D″*) Proof of knockout with Western blot (*B*) and immunofluorescence staining (*C–D″*) with the mTORC1 downstream target P-S6P (green, *C′* and *D′*) and Tamm-Horsfall protein (THP) (red, *C″* and *D″*) as TAL marker in wild-type and *Raptor fl/fl*KspCre* mice. Hoechst 33342 (blue) is the nuclear stain. (Scale bars: 50 µm.) (*E*) *Raptor fl/fl*KspCre* mice showed increased water intake and urinary volume. (*F*) Even after a 12-h thirst challenge, *Raptor fl/fl*KspCre* mice produced a considerable amount of urine. (*G–I*) Urine osmolarity is decreased, whereas plasma osmolarity and urea are increased in *Raptor fl/fl*KspCre* mice. (*J*) Urinary excretion of ADH in *Raptor fl/fl*KspCre* mice is not different from that in wild-type animals, excluding diabetes insipidus. (*K*) In wild-type animals, application of furosemide, but not thiazide or triamterene, could mimic the *Raptor* knockout with regard to urinary flow, loss of body weight, and urinary Ca^{2+} excretion (sampling period after diuretics, 6 h). (*L–N*) Interestingly, despite the application of different types of diuretics, urine osmolarity was practically unchanged in knockout mice, whereas wild-type mice were able to alter their urinary osmolarity depending on the diuretic used. In *E–N*, white bars represent wild-type mice, and black bars represent knockout animals. $^{*}P < 0.05$, $^{**}P < 0.01$, $^{***}P < 0.001$, knockout vs. wild-type; $^{\#}P < 0.05$, $^{\#\#}P < 0.01$, $^{\#\#\#}P < 0.001$, intervention vs. control.

kidney function. To investigate the role of mTORC1 signaling in tubular homeostasis, we characterized tubule-specific constitutive and inducible Cre mice to elucidate the molecular function of mTORC1 in the kidney.

Results

Tubular Cell-Specific mTORC1 Deletion. To eliminate mTORC1 activity in the distal parts of renal tubules, we created *Raptor fl/fl*KspCre* animals (Fig. 1*A*). These constitutive tubule-specific mTORC1-deficient mice were viable and did not show any obvious phenotype up to 4 wk of age. Evaluation of embryonic day (E)12.5 kidney explants in culture revealed no defects in tubular elongation or branching when tissues from wild-type and knockout mice were examined up to E17.5 (Fig. S1). These findings suggest that *KspCre*-mediated mTORC1 deletion is not associated with significant developmental defects. When RAPTOR protein levels were assessed in kidney medulla, a significant reduction could be detected in *Raptor fl/fl*KspCre* animals, as is consistent with the predominant excision of RAPTOR in distal tubular segments (Fig. 1*B*). Because of the tubular epithelial cell-specific approach, some RAPTOR protein was detectable in other tissues not expressing *KspCre*, such as vessels, connective tissue, and *Ksp*$^-$ tubular segments (25). To document further the lack of mTORC1 activity in distal tubular segments, we used Phospho-S6 protein (P-S6P) as an established mTORC1 target in immunofluorescence experiments. The Tamm–Horsfall protein (THP)–positive thick ascending limb of Henle (TAL) of *Raptor fl/fl*KspCre* animals lacked P-S6P reactivity, whereas wild-type animals showed a prominent immunoreactivity (Fig. 1 *C*–*C*″ and *D*–*D*″).

mTORC1 Deficiency Leads to Defective Concentrating Mechanisms and Polyuria. Beginning after weaning, urine production increased in mTORC1-deficient animals, which produced 10 mL urine with a daily water intake of 15 mL (Fig. 1*E*). After a 12-h thirst challenge, urinary flow dropped from 70 μL/h to anuria in wild-type animals, while *Raptor fl/fl*KspCre* animals experienced a reduction of 75% from baseline levels but still produced ∼200 μL/h after the thirst challenge (Fig. 1*F*). Urine osmolality was reduced more than five times, whereas plasma osmolality and plasma urea were increased significantly in knockout animals (Fig. 1 *G*–*I*). Central diabetes insipidus was ruled out by comparable urinary ADH excretion in both genotypes (Fig. 1 *I* and *J*). These findings suggested that *Raptor fl/fl*KspCre* animals display a TAL defect caused by an impaired countercurrent multiplication. Countercurrent multiplication in the TAL is the main driving force of urinary concentration and relies on TAL solute transport from the primary urine into the renal interstitium. In addition, urinary excretion of calcium and magnesium were elevated in knockout mice, pointing to defects in TAL divalent cation reabsorption (Table S1).

For further proof that TAL function is compromised in *Raptor fl/fl*KspCre* animals, we used segment-specific diuretics. Acute i.p. delivery of furosemide, blocking sodium reabsorption in the TAL, decreased the difference in urinary flow between knockout and wild-type animals, whereas administration of either hydrochlorothiazide or triamterene, respectively acting on distal tubules or collecting ducts, increased the difference between the two genotypes (Fig. 1*K*). A similar effect was seen for body weight loss. Only treatment with furosemide caused a comparable weight loss in treated wild-type and *Raptor fl/fl*KspCre* mice (Fig. 1*L*). Furosemide also was the only diuretic that led to similar urinary Ca^{2+} excretion in wild-type and *Raptor fl/fl*KspCre* animals (Fig. 1*M*). Although, as expected, urinary osmolality changed in wild-type mice under diuretic treatment, we observed isosthenuria in *Raptor fl/fl*KspCre* animals (Fig. 1*N*). Taken together, these findings uncover an unexpected role of mTORC1 in fundamentally regulating tubular urine-concentrating mechanisms.

Impaired Mitochondrial Biogenesis in mTORC1-Deficient Tubules. To understand better the observed functional consequences of *KspCre*–driven mTORC1 deficiency, we performed a detailed morphological analysis. On higher magnification, light microscopy sections showed periodic acid Schiff (PAS)-positive inclusion material in TAL cells, detaching and detached tubular cells within tubular lumina, thickened basal membranes, and increased interstitial fibrous tissue (Fig. 2 *A*–*B*′). The increase in fibrous tissue also was seen by immunofluorescence staining for the intermediary filament desmin (Fig. 2 *C*–*D*′) and by acid fuchsin-orange G (SFOG) staining, which revealed increased collagen content (Fig. S1). Silver staining confirmed the thickened basement membranes around TAL sections (Fig. S1). Renal MRI showed a marked hypertrophy of the medulla and papilla in *Raptor fl/fl*KspCre* animals, suggesting an mTORC1-independent compensatory growth mechanism (Fig. S2).

Ultrastructural analysis of wild-type (Fig. 2 *E*–*E*″) and *Raptor fl/fl*KspCre* (Fig. 2 *F*–*F*″) tissues by transmission electron microscopy (TEM) revealed striking abnormalities at the subcellular level. Wild-type TAL cells displayed a high number of long, densely packed mitochondria and numerous basolateral interdigitations enlarging the basolateral cell surface. In contrast mTORC1-deficient TAL cells presented with shortened and fragmented mitochondria, which were irregularly shaped and disordered. The basolateral cell surface appeared reduced, whereas the remaining cytoplasm and nuclei seemed ballooned. The reduced complexity of cytosolic architecture also was seen in principal cells of the collecting duct (CD). These findings provide evidence that *KspCre*-mediated RAPTOR deficiency is associated with a severe mitochondrial defect in the tubular epithelial cells of the TAL and CD.

mTORC1 Transcriptional Networks Regulate Tubular Mitochondrial Metabolism, Transport, and Proliferation. To analyze the mTORC1-dependent tubular functions systematically, we generated transcriptional profiles of five 14-d-old animals of each genotype, using gene set enrichment analysis (GSEA) in combination with the Kolmogorov–Smirnoff test on gene ranks (26). We compared 2,785 gene sets from the Gene Ontology (GO) database for differential regulation. GSEA showed 80 gene sets to be up-regulated and 65 gene sets to be down-regulated between mTORC1-deficient and wild-type animals [false discovery rate (FDR) corrected q-value $<1 \times 10^{-7}$]. The comprehensive network layout of the GSEA analysis is depicted in Fig. 3*A*, in which two nodes (GO terms) are connected if they share at least 20% of their genes. In accordance with the morphological findings, gene sets related to cell division, DNA repair, cell cycle, transcription, and extracellular matrix were up-regulated. In agreement with the functional in vivo data, gene sets linked to transport, mitochondrial metabolism, and mitochondrial biogenesis were significantly down-regulated. Reduced levels of the apical Na^+-K^+-$2Cl^-$ cotransporter (NKCC2) and the thiazide-sensitive sodium-chloride cotransporter (NCC) in cortical and medullary lysates of knockout mice (Fig. 3 *B* and *C*) are a likely explanation for the observed concentrating defect. In contrast, α-ENaC and AQ2 protein levels did not differ between genotypes (Fig. S3 *A* and *B*). In addition, we observed significantly reduced levels of the peroxisome proliferator-activated receptor coactivator alpha (PGC1-α) in *Raptor fl/fl*KspCre* animals (Fig. 3*D*). PGC1-α is a key regulator of mitochondrial biogenesis and is a key downstream target of mTORC1 for control of mitochondrial function in response to nutrient and hormonal signals (27). Although transcriptional programs for peroxisomal and lysosomal processes were down-regulated, mTORC1 deficiency led to distinct transcriptional changes in mTORC2 regulators. These changes included up-regulation of the mTORC2 component PRR5L and down-regulation of the mTORC2 inhibitor DEPTOR, suggesting that mTORC1 deficiency

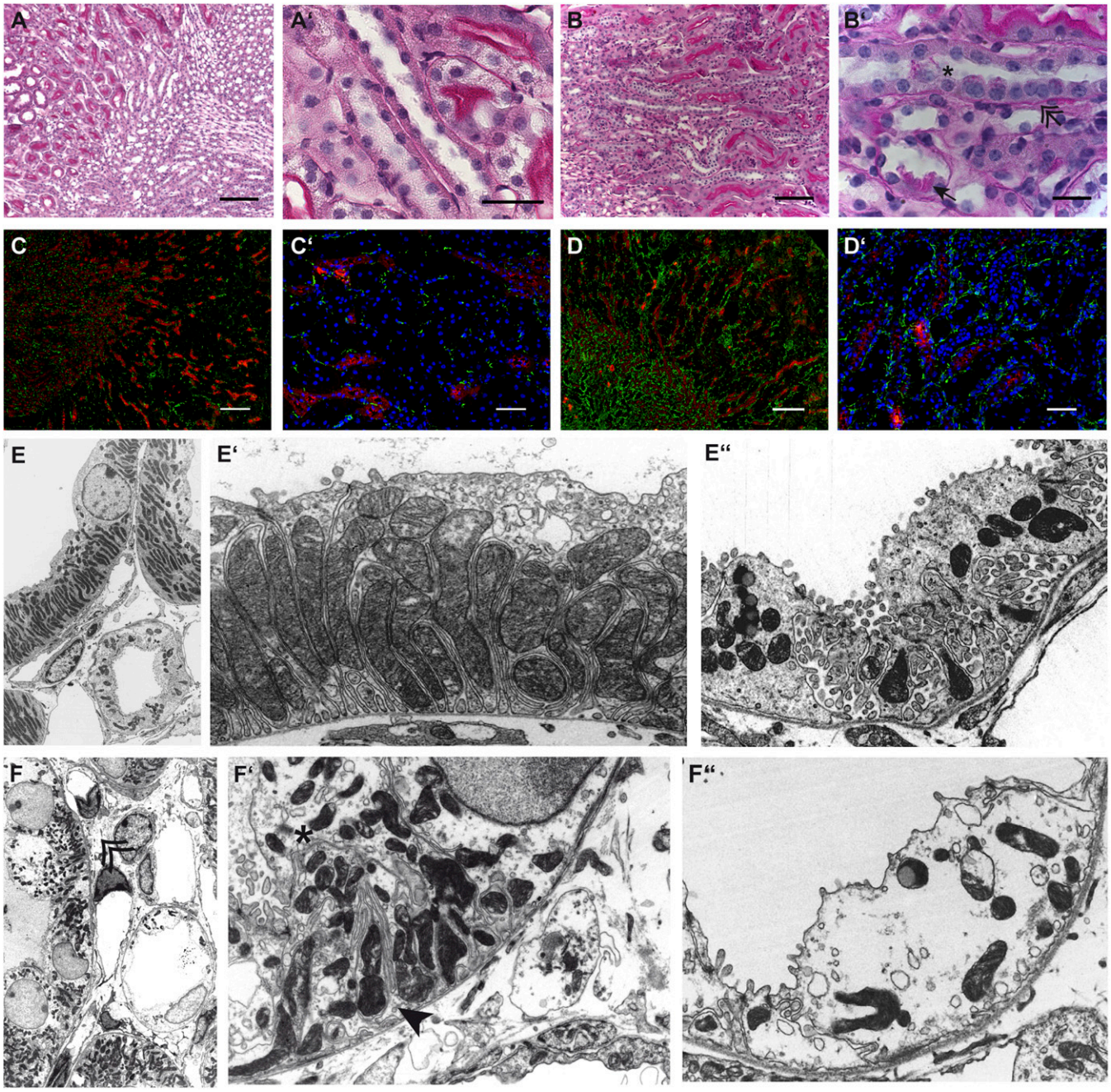

Fig. 2. (*A*–*B*′) PAS-stained sections from wild-type (*A* and *A*′) and knockout (*B* and *B*′) animals showing thickened basement membrane (double arrow), increased connective tissue, and occasional loss of tubular cells (star) with PAS-positive intracellular material (arrow) in knockout mice. (Scale bars: *A*–*D*, 200 μm; *A*′–*D*′, 50 μm; *B*′, 20 μm.) (*C*–*D*′) Desmin (green) and THP (red) staining to assess increased fibrous tissue by immunofluorescence in wild-type (*C* and *C*′) and knockout mice (*D* and *D*′). There is increased deposition of the intermediary filament desmin (green) in both cortex and medulla of knockout animals. (Scale bars: 50 and 200 μm.) (*E*) Electron microscopy of TAL (*E* and *E*′) and CD principal (*E* and *E*′′) cells in wild-type mice showing a normal ultrastructural appearance with palisade-like mitochondria and prominent basolateral interdigitations in the TAL and hill-shaped principal cells with enriched villi and intracellular vesicles in the CD. (*F*–*F*′′) In contrast, *Raptor fl/fl*KspCre* mice have irregularly shaped, shortened mitochondria (star) and only a very few basolateral interdigitations (arrow), whereas CD cells have lost most of their villi and show bigger intracellular vacuoles. Overall, knockout animals show a dramatic increase in fibrous tissue (double arrow). (Magnification: *E* and *F*, 1,500×; *E*′–*F*′′, 4,000×.)

is associated with a compensatory activation of mTORC2 in mTORC1-deficient tubules (Fig. S3*C*).

mTORC2 Deficiency Aggravates the mTORC1-Knockout Phenotype. To evaluate whether mTORC2 partially compensates the deletion of *Raptor*, we generated *Raptor fl/fl*Rictor fl/fl*KspCre* double mutants (Fig. 4*A*). As in mTORC1 single-deficient mice, PS6P signal was absent in TAL segments, confirming the specificity and efficiency of the conditional knockout (Fig. 4 *B* and *C* and Figs. S4 and S5). *Raptor fl/fl*Rictor fl/fl*KspCre* double-mutant mice were born at the expected Mendelian ratio. However, in contrast to *Raptor*-deficient mice, 15% of the double-knockout animals died before reaching adulthood. Thereafter double-mutant mice were significantly smaller than wild-type animals

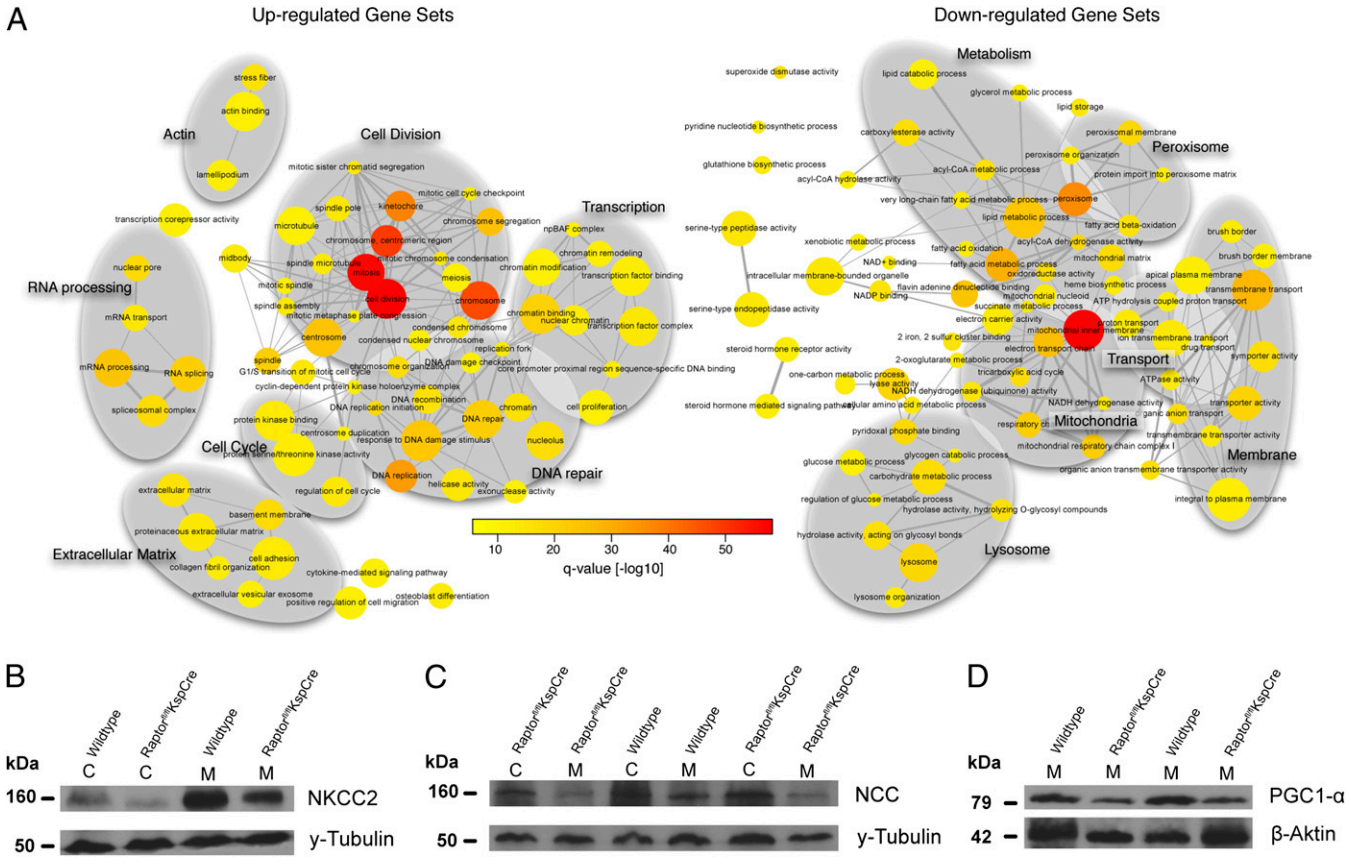

Fig. 3. mTORC1 transcriptional networks regulate tubular mitochondrial metabolism, transport, and proliferation. (*A*) A network representation of a GSEA between *Raptor fl/fl*KspCre* and *Raptor fl/fl* using Gene Ontology gene sets. Nodes correspond to gene sets, which are connected by an edge if they share at least 20% of their genes. Size and color of the nodes are proportional to the size and significance of the gene set. The gray oval backdrops have been added to cluster functionally overlapping gene sets. Gene sets significantly up-regulated in *Raptor*-deficient mice are shown on the left, and gene sets significantly down-regulated in *Raptor*-deficient mice relative to wild-type animals are shown on the right (FDR corrected q-value $<10^{-7}$). (*B* and *C*) Representative Western blots showing reduced abundance of NKCC2 and NCC. (*D*) Expression of PGC1-α, the main regulator of mitochondrial biogenesis, was reduced in medulla of *Raptor fl/fl*KspCre* mice compared with wild-type mice.

and displayed various plasma and urinary changes (Table S2). On gross histologic examination, kidneys from double-knockout mice revealed a condensed papilla and medulla (Fig. 4 *B′*, *B″*, *C′*, and *C″*). Similar to mTORC1-deficient animals, these mice exhibited thickened basement membranes, increased interstitial fibrosis, and loss of cells into the tubular lumen. Most strikingly, TAL cells in the double-knockout mice contained virtually no cytoplasm but had prominent nuclei, giving the tubular sections a pearl necklace-like appearance (Fig. 4 *C″*). Proliferation assessed by Ki-67 staining was increased tremendously, mostly in a peritubular pattern, which corresponded to the increased fibrous tissue content as evidenced by desmin staining (Fig. 4 *D*, *D′*, *E*, and *E′*). To evaluate intercellular connections and integrity, we performed ZO-1 staining, which showed a weblike pattern in wild-type animals but was grossly disrupted, indicating disturbed tubular integrity, in *Raptor fl/fl*Rictor fl/fl*KspCre* animals (Fig. 4 *D″*, *D‴*, *E″*, and *E‴*). These light and immunofluorescent microscopic findings were confirmed by TEM, which revealed ballooned nuclei, detritus-filled tubular lumina, and a dramatic reduction in cytoplasmic organelles in double-knockout animals (Fig. 4 *F* and *F″*). Together these data indicate that mTORC2 cooperates with mTORC1 to maintain normal tubular cell homeostasis and suggest that mTORC2 activity is increased to compensate, in part, for mTORC1 deficiency.

mTORC1 Is Critical for Tubular Ischemic Stress Response. The key role of mTORC1 in tubular energy metabolism suggests that mTORC1 may play an important role during tubular ischemic injury. To circumvent experiments on already structurally altered kidneys and to model the application of mTORC1 inhibitors in a clinical setting more closely, we generated inducible mTORC1-deficient animals, using the *Pax8rtTA*TetOCre* model, which affects all tubular segments (Fig. 5*A*). Treatment with doxycycline was started in *Raptor fl/fl*Pax8rtTA*TetOCre* mice 2 wk before I/R injury to the left kidney and was continued until the animals were killed. Light microscopy of PAS-stained sections taken before I/R did not reveal any differences between wild-type and knockout mice (Fig. 5 *B* and *C*). Twenty-four hours after I/R injury, cell sloughing, cell flattening, and distal tubular cast formation were more severe in *Raptor fl/fl*Pax8rtTA*TetOCre* animals than in their wild-type littermates (Fig. 5 *D–E′*). Mitochondria appeared normal in knockout animals not exposed to I/R injury, suggesting that gene excision generally is well tolerated in adult animals, at least in the short term. However, we observed an increased number of multilamellar bodies in proximal tubular cells of knockout mice, indicating disturbed cellular recycling mechanisms (Fig. 5 *F–G″*). Following I/R injury, increased damage was evident in kidney sections stained for cleaved caspase 3 (cCASP3), a marker for apoptotic cells, and evaluated using a blinded, semiautomated scanning and counting algorithm (Fig. 5*H*). cCASP3$^+$ cells were increased by approximately threefold in knockout mice after I/R, although the two genotypes were not different under control conditions (Fig. 5*I*). Furthermore, *Raptor fl/fl*Pax8rtTA*TetOCre* animals

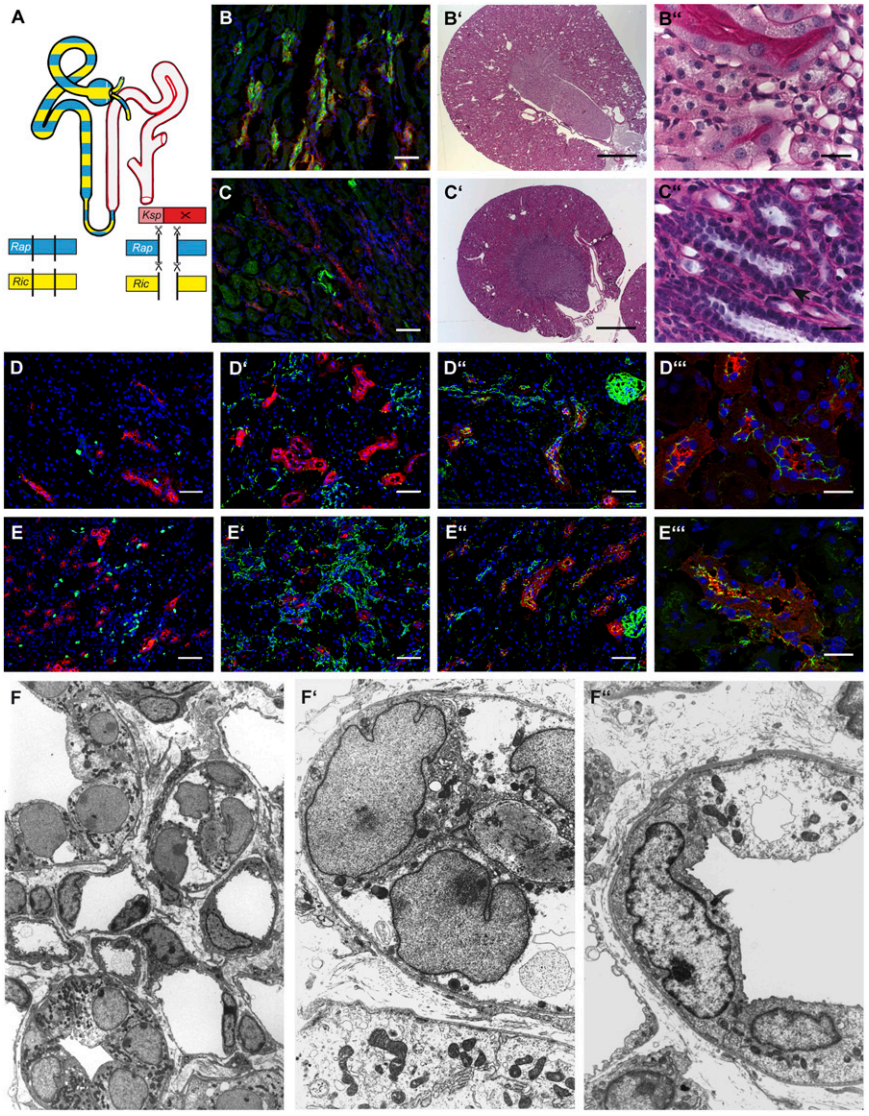

Fig. 4. mTORC2 deficiency aggravates the mTORC1-knockout phenotype. (*A*) Schematic of the recombination strategy and site of knockout within the tubular system. (*B* and *C*) Immunofluorescence evidence (red, THP; green, P-S6P; blue, Hoechst 33342) that the well-known mTORC1 downstream target P-S6 protein is not phosphorylated in knockout animals, demonstrating functional knockout of mTORC1. (*B′* and *B″*) Wild-type tissue at two different magnifications showing normal renal tissue with no obvious architectural or histological abnormalities, especially in the medullo-papillary region. (*C′* and *C″*) Macroscopically abnormal renal tissue of a knockout littermate, showing condensed medullo-papillary tissue, broad basal membranes, increased interstitial fibrosis, prominent nuclei, and lack of cellular plasma (arrow). In addition, detached cells can be visualized within the tubular lumen. (*D*, *D′*, *E*, and *E′*) Increased proliferation (*D* and *E*: red, THP; green, Ki-67; blue, Hoechst 33342) as well as elevated fibrous tissue (*D′* and *E′*: green, desmin; red, THP; blue Hoechst 33342) within renal tissue of *Raptor fl/fl*Rictor fl/fl*KspCre* mice. (*D″*, *D‴*, *E″*, and *E‴*) Destroyed intercellular connections between THP^+ (red) TAL cells as evidenced by fragmented ZO-1 staining (green) in tissue from a knockout mouse. (Scale bars: *B*, *B″*, *C*, *C″*, *D*–*D″*, and *E*–*E″*, 50 μm; *B′* and *C′*, 1,000 μm; *D‴* and *E‴*, 20 μm.) (*F*–*F″*) Electron microscopy shows ultrastructural damage with dramatically shifted cytoplasm/nucleus ratios, debris-filled tubular lumina (white star), thickened basement membranes, and increased fibrous tissue. (Magnification: *F*, 1,200×; *F′* and *F″*, 4,000×.)

showed a significantly reduced proliferative response after I/R injury. Ki-67^+ nuclei in knockout animals were reduced by ∼2.5-fold compared with wild-type animals at 48 and 72 h post I/R (Fig. 5 *H* and *I*). Functionally, urinary neutrophil gelatinase-associated lipocalin (NGAL) levels were strikingly higher in *Raptor fl/fl*Pax8rtTA*TetOCre* mice than in wild-type animals (Fig. 5*J*). Thus, lack of mTORC1 function results in dramatically accelerated tubular injury and apoptosis and prevents the proliferative response that usually facilitates renal repair and regeneration after tubular injury.

Discussion

Despite its original discovery more than 20 y ago and its recognition as a central regulator of protein and lipid synthesis, lysosome biogenesis, energy metabolism, autophagy, and cell survival, our understanding of many functions of the mTOR complex is still evolving (13). Although inhibitors of mTORC1 are used in solid-organ transplantation and increasingly are used in other human diseases, relatively little is known about the role of mTORC1 in normal kidney homeostasis. This deficit limits our ability to anticipate the renal side effects and toxicities of mTOR inhibition. Using constitutive- and inducible-knockout models with the ability to eliminate mTORC1 and/or mTORC2 selectively in renal tubular epithelial cells, our study uncovered crucial functions of mTORC1 in tubular mitochondrial biogenesis, urine-concentrating mechanisms, and response to ischemic injury. *Raptor fl/fl*KspCre* mice presented with polyuria and polydipsia. Because the *Ksp* promoter-mediated *Raptor* excision primarily targets the TAL and distal tubules, a nonfunctional counter-current-concentrating mechanism in the TAL and/or renal diabetes insipidus in the CD could explain the observed phenotype (28, 29). We did not observe increased urinary ADH secretion or decreased renal AQ2 protein levels but instead observed increased urinary Ca^{2+} and Mg^{2+} excretion and a compensatory increase in plasma urea, so a defective counter-current mechanism appeared to be the most likely explanation. Gene-expression profiling revealed decreased expression of PGC1-α. Because PGC1-α is responsible for mitochondrial biogenesis (27, 30), this finding implies that mTORC1 deficiency or inhibition interferes with normal mitochondrial biogenesis in tubular epithelial cells. The transcriptional network analysis also revealed that mTORC1 deficiency not only impairs energy provision for ion transporters but also directly affects the expression of key transporters, such as NKCC2, that are responsible for sodium reabsorption in the TAL. Consistent with a transport defect in the TAL, *Raptor fl/fl*KspCre* mice could concentrate their urine only partially after a 12-h thirst challenge. The response to furosemide was

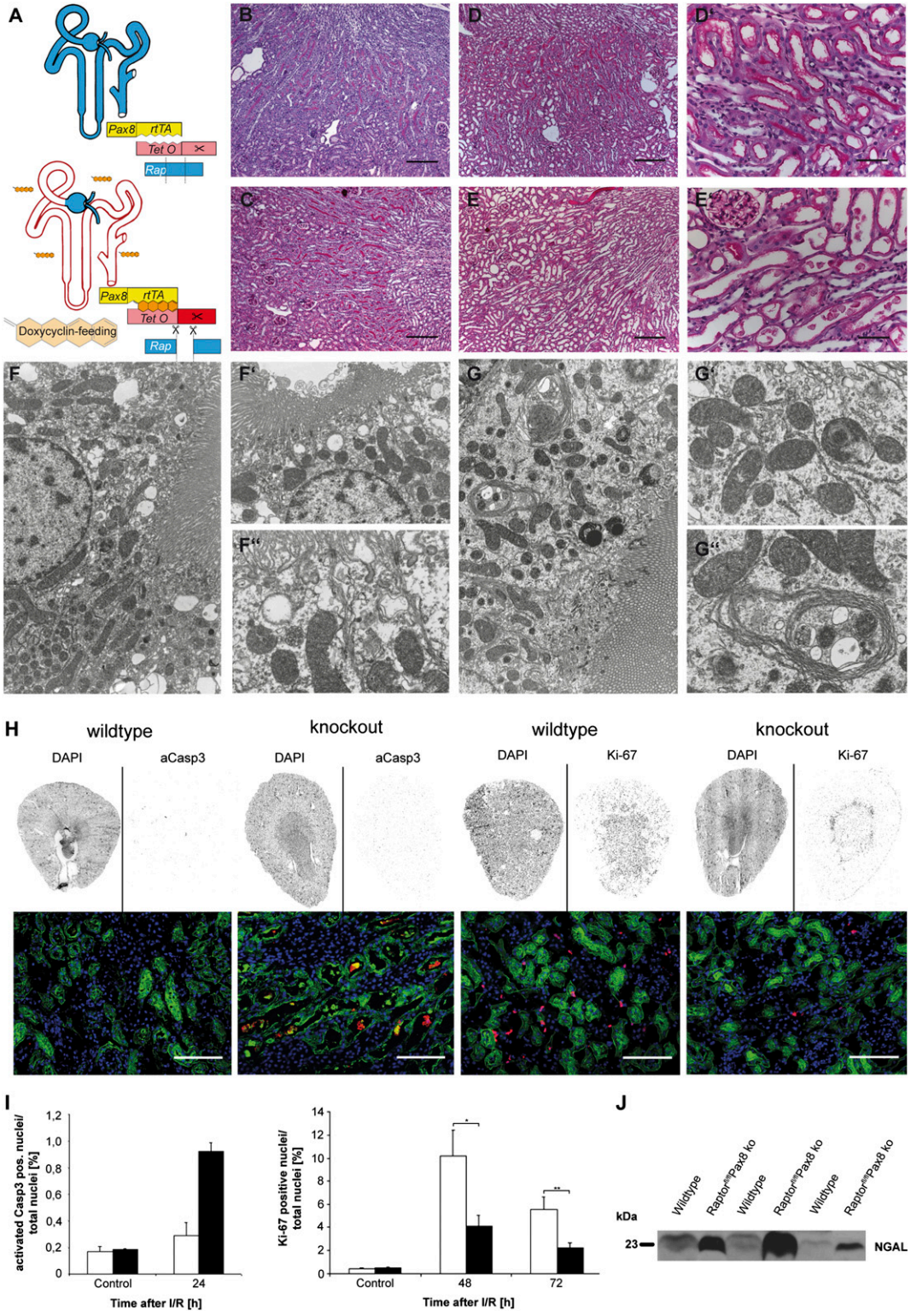

Fig. 5. mTORC1 is critical for the tubular ischemic stress response. (*A*) Inducible recombination scheme with doxycycline. (*B* and *C*) Histology of unstressed wild-type (*B*) and knockout (*C*) mice with no obvious phenotype. (*D–E′*) After I/R there is widespread damage, especially in proximal tubules, which is more pronounced in knockout (*E* and *E′*) than in wild-type (*D* and *D′*) animals. (*F–F″*) Normal ultrastructure of proximal tubular cells with brush border, mitochondria, and endocytic vacuoles. (*G–G″*) Knockout mice present with multilamellar bodies and apparently reduced endocytosis but do not show an obvious mitochondrial defect. (Magnification: *F* and *G*, 4,000×; *F′*, 6,000×; *F″*, *G′*, and *G″*, 10,000×.) (*H* and *I*) Renal arteries were clamped for 30 min, and kidneys were harvested 24, 48, and 72 h after reperfusion. The increased apoptosis indicated by cCASP3$^+$ cells (red) in knockout animals was assessed reliably by a semiautomated approach using slices of whole kidney. In contrast, when the same semiautomated evaluation method was used, proliferation, as assessed by Ki-67$^+$ nuclei (red), was higher in wild-type animals than in knockout animals. Lotus Tetragonobulus (peanut lectin) (green) is the marker for proximal tubules, and Hoechst 33342 (blue) was used to stain nuclei. (Scale bars: *B*, *C*, *D*, and *E*, 200 μm; *D′*, *E′*, and *H*, 50 μm.) (*J*) Urinary Western blots adjusted for creatinine concentration discern a much higher NGAL concentration in knockout animals, indicating more severe acute renal injury in this group.

reduced in *Raptor fl/fl*KspCre* mice, supporting our hypothesis that mTORC1 deficiency in the TAL affects the transport-dependent countercurrent-concentration mechanism. Morphological analysis of the TAL in *Raptor*-deficient mouse kidneys revealed that mitochondria of the tubular epithelial cells were reduced and fragmented and that the basolateral surface area was strikingly reduced.

We speculated that mTORC2 might partially compensate the loss of TORC1 in the renal tubular apparatus (31), because *Raptor fl/fl*Rictor fl/fl*KspCre* double mutants lacking both mTORC1 and mTORC2 activity showed a more severe phenotype, and 15% of these animals died during adolescence because of profound disturbances in water and electrolyte balance. Furthermore, mTORC2 deficiency alone did not show any morphological or functional abnormalities under baseline conditions, suggesting that mTORC2 partially compensates for and reduces pathophysiological disturbances caused by RAPTOR/mTORC1 deficiency, potentially by increasing AKT prosurvival signaling (32, 33).

The proximal tubule probably is the most energy-consuming nephron segment with the highest abundance of mitochondria; this segment is not targeted by the *Ksp* promoter (4, 5, 25, 34). Because of its high oxygen consumption, it is very vulnerable during I/R injury of the kidney. To address the role of mTORC1 in the proximal kidney tubules in response to ischemia, we used the doxycycline-inducible *Pax8rtTa*TetOCre* system to target all tubular cells (35). In the first 24 h after I/R injury *Raptor fl/fl*Pax8rtTa*TetOCre* animals showed higher urinary levels of NGAL and a threefold higher rate of apoptotic cells, demonstrating that mTORC1 deficiency increases the susceptibility of proximal tubular cells to ischemic injury. This finding is in line with a recent report demonstrating reduced cytoprotective capacity under everolimus treatment in I/R in rats (36). In the 48 h after I/R, mTORC1-deficient tubules showed a reduced proliferative response, corresponding with the documented delayed graft function in kidney transplant patients treated with mTORC1 inhibitors (20, 21).

In summary, our data highlight a fundamental role of mTOR signaling in tubular epithelial cell function in health and disease. The mTOR-driven mitochondrial energy supply and mTOR-dependent transcriptional regulation of ion transport channels act synergistically to maintain the TAL-based countercurrent-concentrating mechanism. Although mTORC2 might contribute partially to renal epithelial cell homeostasis, mTORC1 is critical for protecting cells against apoptosis and facilitating their recovery in response to acute ischemic kidney injury.

Materials and Methods

Animals. All animal experiments were conducted according to the National Institutes of Health *Guide for the Care and Use of Laboratory Animals* (37), as well as the German law governing the welfare of animals, and were approved by the respective Regierungspräsidium (G-10/39 and M-9/11). Mice were housed in a specific pathogen-free facility with free access to chow and water and a 12-h day/night cycle. Breeding and genotyping were done according to standard procedures. *Raptor fl/fl* mice have been described previously (38) and were crossed to *KspCre* (25) or *Pax8rtTA* (35) and *TetOCre* (39) animals. Beginning at age 5 wk, inducible animals and respective controls (lacking either *TetoCre* or *Pax8rtTA*) received doxycycline hydrochloride (Fagron) via the drinking water (2 mg/mL with 5% (wt/vol) sucrose, protected from light) for 14 d before I/R kidney injury; the drug was continued until the animals were killed. For I/R injury, mice were anesthetized with ketamine/xylazine [120 μg/ and 8 μg/g body weight (bw), respectively] and were kept under infrared light to maintain body temperature. After the administration of deep anesthesia, an incision was made in the left flank, the left kidney was mobilized, and the kidney artery was clamped for 30 min. After reperfusion, 0.9% NaCl (40 μL/g bw) was given i.p., internal wounds were closed with Vicryl 5–0 (Ethicon), and the skin was stapled. Adequate pain relief was given after mice regained consciousness. Mice were killed after urine collections were taken 24, 48, or 72 h after I/R. The upper half of the left kidney was snap frozen for immunofluorescence, and the lower half of that kidney was perfusion-fixed with 4% (wt/vol) paraformaldehyde in phosphate buffer for further histologic evaluation. The right kidney served as an internal control.

To study renal excretion, mice were studied in metabolic cages for 2 d on a control diet (C1000; Altromin) and tap water followed by a 12-h period of water deprivation. The response to different diuretics was studied by i.p. injection of furosemide (20 μg/g bw), hydrochlorothiazide (20 μg/g bw), or triamterene (20 μg/g bw) (all drugs from Sigma) followed by 6-h period without access to water and food during which urine was collected. Control experiments were performed with vehicle (5 μL/g bw of 2.5% vol/vol DMSO in injectable water) (40). Blood samples under control conditions were drawn by puncturing the right retro-orbital plexus under isoflurane anesthesia 14 d after the experiments in the metabolic cages.

Measurements. Plasma concentrations of Na^+, K^+, and Ca^{2+} were measured by flame photometry (EFUX 5057; Eppendorf). Plasma and urinary magnesium and phosphorus concentrations were determined by colorimetric methods (Lehmann). Plasma aldosterone concentration and urinary vasopressin were measured using radioimmunoassay kits (Demeditec). Serum and urinary osmolality were determined using an osmometer based on the freezing point depression method (Knauer). Venous blood gas analysis was done using a Gem Premier 3000 analyzer (Instrumentation Laboratory). Urinary and serum creatinine and urea were measured using enzymatic colorimetric creatinine and urea kits (Lehmann) following the manufacturer's instructions. Urinary NGAL was determined using analysis of urinary Western blots with a mouse NGAL-specific antibody (R&D Systems).

Transcriptome Analysis. *Raptor fl/fl*KspCre* and *Raptor fl/fl* animals were killed at postnatal day 14 before the development of an overt functional phenotype. Kidneys were split in half and snap frozen immediately in liquid nitrogen. RNA was purified using standard procedures and analyzed using the Affimetrix Mouse 4302 chip. Raw data were obtained by standard array hybridization techniques and normalized via the Single Channel Array Normalization algorithm (41) mapping the probes to the custom chip definition file from the BrainArray resource (http://brainarray.mbni.med.umich.edu/Brainarray/Database/CustomCDF/) in version 17 (42). Pathway analyses were performed using the generally applicable GSEA, GAGE, which determines whether a set of genes is systematically up- or down-regulated as a whole, although individual genes need not be significantly regulated (26). For gene set definitions we used the gene ontology provided with the org.Mm.eg.db genome-wide annotation package for mouse (Bioconductor, version 2.9). We discarded gene sets having less than 10 or more than 500 members, thus reducing the number of analyzed gene sets to 2,785. To assess the significance of differential regulation, we used a gene rank-based nonparametric Kolmogorov–Smirnoff test, which makes no assumption about the underlying distribution of the data, thereby increasing the detection sensitivity. Raw GSEA *P* values were corrected for multiple testing assuming an FDR threshold of significance up to 1×10^{-7}. Transcriptomic datasets are available at the Gene Expression Omnibus database under accession no. GSE54417.

Morphological Analysis. Kidneys were perfusion fixed in 4% phosphate-buffered paraformaldehyde, embedded in paraffin, and further processed for PAS, SFOG, or silver staining. For ultrastructural analysis kidneys also were fixed in 4% (wt/vol) paraformaldehyde in phosphate buffer. Samples were postfixed in 1% osmium tetroxide in the same buffer for 1 h and stained *en bloc* in 1% uranyl acetate in 10% (vol/vol) ethanol for 1 h, dehydrated in ethanol, and embedded in LX112 resin (Thermo Fisher). Semithin sections were stained with toluidine blue. Thin sections were stained with uranyl acetate and lead citrate and were examined in a Jeol JEM 1200EX electron microscope.

Western Blot. Kidneys were glass-homogenized in lysis buffer containing 20 mM CHAPS and 1% Triton X-100. After centrifugation (15,000 × *g* for 15 min at 4 °C), protein concentration was determined by the DC Protein Assay (Bio-Rad). Equal amounts of protein were separated on SDS/PAGE.

Immunofluorescence Staining of Kidney Sections. Kidneys were frozen in Optimum Cutting Temperature (O.C.T.) compound and sectioned at 5 μm (Leica Kryostat). The sections were fixed with 4% paraformaldehyde, blocked in PBS containing 5% BSA plus 5% normal donkey serum, and incubated for 45 min with primary antibodies as indicated. After several PBS rinses, fluorophore-conjugated secondary antibodies (Life Technologies) were applied for 30 min. Images were taken using a Zeiss fluorescence microscope equipped with 20× and 63× water immersion objectives (Zeiss).

Semiautomated Assessment of Proliferation and Apoptosis. Kidneys were cut and stained as outlined above with Ki-67 (Thermo Scientific) and activated caspase 3 antibodies (Cell Signaling). Three sections 150 μm apart were taken from each kidney. Images of the whole kidney slice were recorded on a Zeiss fluorescence microscope with a 10× objective on a motorized stage hooked up to the Axiovision software including the plug-in MosaiX (Zeiss). Individual pictures were stitched and converted into a tile image thaat was used for further analysis. Ki-67 and activated caspase 3-positive nuclei were analyzed by Image J and its plug-in Nucleus Counter (http://rsb.info.nih.gov/ij/index.html).

MRI Measurement of Cortex and Medulla. Imaging experiments were carried out on a 9.4-T (400 MHz) horizontal magnet (Bruker Biospin). A quadrature birdcage coil (Bruker Biospin) with an inner diameter of 38 mm was used. The mice were anesthetized with isoflurane, and breathing rate and heart rate were monitored by ECG to ensure that they remained at a constant level. Cardiac gating was used to reduce motion artifacts caused by respiration and blood flow.

The mice were placed horizontally in the prone position on the x–z plane with their anteroposterior direction along the coil axis, z. The imaging protocol consisted of the following sequences: A localizer was used for morphological reference. A fluid-sensitive T2-weighted spin echo rapid acquisition with relaxation enhancement sequence was performed to delineate the renal cortex, medulla, and the pelvis (TR/TEeff/FA: 3,000 ms/36 ms/180°; echo train length, 8). The sequence featured a 30 × 30 mm field of view, a matrix size of 256 ×256 pixels, and an in-plane resolution of 117 × 117 mm. The slice thickness was 0.5 mm with no slice spacing to achieve contiguous image sets of the whole volume.

Morphological analyses were performed using Medical Image Processing and Visualization (MIPAV) software freely available from the National Institutes of Health. The renal pelvic volume and the parenchymal index (PI, defined as the diameter of the renal mark versus the total renal parenchyma, measured orthogonally to the longitudinal axis of the kidney opposite to the hilum) were recorded. To determine the total renal pelvis volume, the perimeter of the pelvis, which could be clearly distinguished from the surrounding parenchyma, was traced manually on each slice image. The total volume of the pelvis was calculated from sets of contiguous images by summing up the products of area measurements and slice thickness using the volume of interest (VOI) tool in MIPAV. The total renal volume was determined similarly, delineating the kidney versus the surrounding tissue.

Metanephric Kidney Culture. Timed matings were set up with male *Raptor fl/fl* and female *Raptor fl/fl*KspCre* mice; the date of the vaginal plug was designated as day 0.5. Metanephric kidneys were microdissected from the embryos at E12.5 and cultured in DMEM containing 10% FCS and 1% penicillin and streptomycin at 37 °C and 5% CO_2 on 0.4-μm Transwell inserts (43). The medium was replaced every 48 h. The kidney cultures were harvested after 5 d in culture. For whole-mount immunofluorescence staining, the cultures were fixed in methanol, blocked in BSA, and stained with primary and secondary antibodies overnight (44).

Antibodies. The following antibodies were used: rabbit anti-RAPTOR, rabbit anti-PhosphoS6, and rabbit anti-totalS6 (Cell Signaling); rabbit anti-NKCC2, rabbit anti-NCC, and rabbit anti-alphaENaC (StressMarq Biosciences Inc.); rabbit anti–Ki-67 (Thermo Fisher Scientific); rabbit anti–PGC1-alpha (Abcam); Hoechst 33342 and mouse anti–ZO-1 (Life Technologies); rabbit anti-active caspase 3 and goat anti-NGAL (R&D Systems); sheep anti-THP (AbdSerotec); mouse anti-desmin (Sigma-Aldrich); rabbit anti-AQ2 (Alomone Lab); mouse anti–Pan-cytokeratin (Biozol Diagnostica); and mouse anti- CALBINDIN D28K (Swant).

Statistics. Data are expressed as mean ± SEM. Statistical comparisons were performed using GraphPad Prism Software Package 6 (GraphPad Software Inc.) with a two-tailed Student t test or ANOVA, including respective corrections where indicated. Differences with P values greater than 0.05 were considered significant.

ACKNOWLEDGMENTS. We thank Betina Kiefer, Charlotte Meyer, Temel Kilic, Helga Schachner, Evelyn Wätzig, and Annette Merkle for expert technical assistance and all members of our laboratories for helpful discussions and support. This study was supported by grants from Deutsche Forschungsgemeinschaft (DFG) "Polycystic Kidney Disease–From Model Organisms to Novel Therapies" (KFO 201) (to F.G., W.R., G.W., and T.B.H.), DFG Heisenberg Program (to T.B.H.), and Collaborative Research Center 992 (to T.B.H.); by European Research Council Grant Project DNCure (to T.B.H.); by the Excellence Initiative of the German Federal and State Governments (EXC294, to T.B.H.; GSC-4) Spemann Graduate School (to N.W. and T.B.H.); by the Federal Ministry of Education and Research Joint Transnational Grant 01KU1215 (to T.B.H.) and GerontoSys2-Project NephAge (to H.B., M.B., and T.B.H.); and by project-specific grant support by Pfizer Pharma GmbH (formerly Wyeth GmbH) (to T.B.H.).

1. Greger R (2000) Physiology of renal sodium transport. *Am J Med Sci* 319(1):51–62.
2. Hoorn EJ, Nelson JH, McCormick JA, Ellison DH (2011) The WNK kinase network regulating sodium, potassium, and blood pressure. *J Am Soc Nephrol* 22(4):605–614.
3. Mercier-Zuber A, O'Shaughnessy KM (2011) Role of SPAK and OSR1 signalling in the regulation of NaCl cotransporters. *Curr Opin Nephrol Hypertens* 20(5):534–540.
4. Mandel LJ, Balaban RS (1981) Stoichiometry and coupling of active transport to oxidative metabolism in epithelial tissues. *Am J Physiol* 240(5):F357–F371.
5. Mandel LJ (1986) Primary active sodium transport, oxygen consumption, and ATP: Coupling and regulation. *Kidney Int* 29(1):3–9.
6. Soltoff SP (1986) ATP and the regulation of renal cell function. *Annu Rev Physiol* 48: 9–31.
7. Wullschleger S, Loewith R, Hall MN (2006) TOR signaling in growth and metabolism. *Cell* 124(3):471–484.
8. Heitman J, Movva NR, Hall MN (1991) Targets for cell cycle arrest by the immunosuppressant rapamycin in yeast. *Science* 253(5022):905–909.
9. Sarbassov DD, et al. (2004) Rictor, a novel binding partner of mTOR, defines a rapamycin-insensitive and raptor-independent pathway that regulates the cytoskeleton. *Curr Biol* 14(14):1296–1302.
10. Jacinto E, et al. (2004) Mammalian TOR complex 2 controls the actin cytoskeleton and is rapamycin insensitive. *Nat Cell Biol* 6(11):1122–1128.
11. Kim DH, et al. (2002) mTOR interacts with raptor to form a nutrient-sensitive complex that signals to the cell growth machinery. *Cell* 110(2):163–175.
12. Hara K, et al. (2002) Raptor, a binding partner of target of rapamycin (TOR), mediates TOR action. *Cell* 110(2):177–189.
13. Laplante M, Sabatini DM (2012) mTOR signaling in growth control and disease. *Cell* 149(2):274–293.
14. Peterson TR, et al. (2011) mTOR complex 1 regulates lipin 1 localization to control the SREBP pathway. *Cell* 146(3):408–420.
15. Golbaekdal K, Nielsen CB, Djurhuus JC, Pedersen EB (1994) Effects of rapamycin on renal hemodynamics, water and sodium excretion, and plasma levels of angiotensin II, aldosterone, atrial natriuretic peptide, and vasopressin in pigs. *Transplantation* 58(11):1153–1157.
16. Haller M, et al. (2012) Sirolimus induced phosphaturia is not caused by inhibition of renal apical sodium phosphate cotransporters. *PLoS ONE* 7(7):e39229.
17. Morales JM, et al. (2003) Tubular function in patients with hypokalemia induced by sirolimus after renal transplantation. *Transplant Proc* 35(3, Suppl):154S–156S.
18. Morales JM, et al.; Sirolimus European Renal Transplant Study Group (2002) Sirolimus does not exhibit nephrotoxicity compared to cyclosporine in renal transplant recipients. *Am J Transplant* 2(5):436–442.
19. Kempe DS, et al. (2010) Rapamycin-induced phosphaturia. *Nephrol Dial Transplant* 25(9):2938–2944.
20. Smith KD, et al. (2003) Delayed graft function and cast nephropathy associated with tacrolimus plus rapamycin use. *J Am Soc Nephrol* 14(4):1037–1045.
21. Lieberthal W, Fuhro R, Andry C, Patel V, Levine JS (2006) Rapamycin delays but does not prevent recovery from acute renal failure: Role of acquired tubular resistance. *Transplantation* 82(1):17–22.
22. Bissler JJ, et al. (2013) Everolimus for angiomyolipoma associated with tuberous sclerosis complex or sporadic lymphangioleiomyomatosis (EXIST-2): A multicentre, randomised, double-blind, placebo-controlled trial. *Lancet* 381(9869):817–824.
23. Hudes G, et al.; Global ARCC Trial (2007) Temsirolimus, interferon alfa, or both for advanced renal-cell carcinoma. *N Engl J Med* 356(22):2271–2281.
24. Baselga J, et al. (2012) Everolimus in postmenopausal hormone-receptor-positive advanced breast cancer. *N Engl J Med* 366(6):520–529.
25. Shao X, Somlo S, Igarashi P (2002) Epithelial-specific Cre/lox recombination in the developing kidney and genitourinary tract. *J Am Soc Nephrol* 13(7):1837–1846.
26. Luo W, Friedman MS, Shedden K, Hankenson KD, Woolf PJ (2009) GAGE: Generally applicable gene set enrichment for pathway analysis. *BMC Bioinformatics* 10:161.
27. Cunningham JT, et al. (2007) mTOR controls mitochondrial oxidative function through a YY1-PGC-1alpha transcriptional complex. *Nature* 450(7170):736–740.
28. Takahashi N, et al. (2000) Uncompensated polyuria in a mouse model of Bartter's syndrome. *Proc Natl Acad Sci USA* 97(10):5434–5439.
29. Devuyst O (2012) Physiopathology and diagnosis of nephrogenic diabetes insipidus. *Ann Endocrinol (Paris)* 73(2):128–129.
30. Schieke SM, et al. (2006) The mammalian target of rapamycin (mTOR) pathway regulates mitochondrial oxygen consumption and oxidative capacity. *J Biol Chem* 281(37):27643–27652.
31. Guertin DA, et al. (2006) Ablation in mice of the mTORC components raptor, rictor, or mLST8 reveals that mTORC2 is required for signaling to Akt-FOXO and PKCalpha, but not S6K1. *Dev Cell* 11(6):859–871.
32. Canaud G, et al. (2013) AKT2 is essential to maintain podocyte viability and function during chronic kidney disease. *Nat Med* 19(10):1288–1296.
33. Gödel M, et al. (2011) Role of mTOR in podocyte function and diabetic nephropathy in humans and mice. *J Clin Invest* 121(6):2197–2209.
34. Brooks C, Wei Q, Cho SG, Dong Z (2009) Regulation of mitochondrial dynamics in acute kidney injury in cell culture and rodent models. *J Clin Invest* 119(5):1275–1285.
35. Traykova-Brauch M, et al. (2008) An efficient and versatile system for acute and chronic modulation of renal tubular function in transgenic mice. *Nat Med* 14(9): 979–984.

36. Kezic A, Thaiss F, Becker JU, Tsui TY, Bajcetic M (2013) Effects of everolimus on oxidative stress in kidney model of ischemia/reperfusion injury. *Am J Nephrol* 37(4): 291–301.
37. Committee on Care and Use of Laboratory Animals (1985) *Guide for the Care and Use of Laboratory Animals* (Natl Inst Health, Bethesda), DHHS Publ No (NIH) 85-23.
38. Bentzinger CF, et al. (2008) Skeletal muscle-specific ablation of raptor, but not of rictor, causes metabolic changes and results in muscle dystrophy. *Cell Metab* 8(5): 411–424.
39. Eremina V, et al. (2008) VEGF inhibition and renal thrombotic microangiopathy. *N Engl J Med* 358(11):1129–1136.
40. Artunc F, et al. (2009) Responses to diuretic treatment in gene-targeted mice lacking serum- and glucocorticoid-inducible kinase 1. *Kidney Blood Press Res* 32(2):119–127.
41. Piccolo SR, et al. (2012) A single-sample microarray normalization method to facilitate personalized-medicine workflows. *Genomics* 100(6):337–344.
42. Dai M, et al. (2005) Evolving gene/transcript definitions significantly alter the interpretation of GeneChip data. *Nucleic Acids Res* 33(20):e175.
43. Avner ED, Villee DB, Schneeberger EE, Grupe WE (1983) An organ culture model for the study of metanephric development. *J Urol* 129(3):660–664.
44. Gao X, et al. (2005) Angioblast-mesenchyme induction of early kidney development is mediated by Wt1 and Vegfa. *Development* 132(24):5437–5449.